Hydrogen bond spectroscopy in the near infrared: Outofplane torsion and antigeared bend combination bands in (HF)2

David T. Anderson, Scott Davis, and David J. Nesbitt

Citation: The Journal of Chemical Physics **105**, 4488 (1996); doi: 10.1063/1.472293
View online: http://dx.doi.org/10.1063/1.472293
View Table of Contents: http://scitation.aip.org/content/aip/journal/jcp/105/11?ver=pdfcov
Published by the AIP Publishing

Hydrogen bond spectroscopy in the near infrared: Out-of-plane torsion and antigeared bend combination bands in $(HF)_2$

David T. Anderson,[a] Scott Davis, and David J. Nesbitt[b]
JILA, University of Colorado and National Institute of Standards and Technology, and Department of Chemistry and Biochemistry, University of Colorado, Boulder, Colorado 80309-0440

(Received 25 March 1996; accepted 28 May 1996)

High-resolution near infrared spectra of the two ''high'' frequency intermolecular modes of $(HF)_2$ have been characterized in HF-stretch excited states using a slit jet spectrometer. In the spectral region between 4280 and 4480 cm^{-1}, four vibration–rotation–tunneling (VRT) bands are observed and assigned to tunneling pairs of the out-of-plane torsion (ν_6) and antigeared bend (ν_3) intermolecular modes, in combination with the hydrogen bond donor (ν_2) and acceptor (ν_1) high-frequency intramolecular HF stretches, respectively. Analysis of the jet-cooled, rotationally resolved spectra provide intermolecular frequencies, rotational constants, tunneling splittings, and predissociation rates for the ν_3/ν_6 intermolecular excited states. The relatively small changes in the hydrogen bond interconversion tunneling splitting with either ν_3 or ν_6 excitation indicate that neither intermolecular mode is strongly coupled to the tunneling coordinate. The high-resolution VRT linewidths reveal mode specific predissociation broadening sensitive predominantly to *intramolecular* excitation, but with significant additional effects due to low-frequency *intermolecular* excitation as well. The intermolecular vibrational frequencies in the combination states display a systematic dependence on intramolecular redshift that allows all four intermolecular fundamental frequencies to be extrapolated from the near-ir data. Agreement between full 6-D quantum calculations and experiment for the out-of-plane torsion (ν_6) vibration is remarkably good (0.5%). However, significant discrepancies (>10%) between theory and experiment are obtained for the antigeared bend (ν_3), indicating the need for further refinement of the HF dimer potential surface. Finally, the observation of all four intermolecular modes allows zero-point contributions to the binding energy to be reliably estimated. The revised value for the binding energy, $D_e=1580(35)$ cm^{-1}, is slightly higher than semiempirical estimates but now in excellent agreement with recent high level *ab initio* calculations. © *1996 American Institute of Physics.* [S0021-9606(96)02733-X]

I. INTRODUCTION

The hydrogen fluoride dimer $(HF)_2$ has long served as a simple molecular paradigm for detailed study of hydrogen bonding properties. $(HF)_2$ is particularly attractive both from an experimental and theoretical point of view, due to the limited number of internal degrees of freedom (6-D) and total electron count (20). An extensive succession of high-resolution spectroscopic studies of $(HF)_2$ in the microwave,[1–4] far-ir,[5–8] and near-ir[9–19] spectral regions have led to accurate determination of vibrationally averaged structural parameters, interconversion tunneling rates, intramolecular vibrational frequencies, photofragment rotational distributions, and the hydrogen bond dissociation energy (D_0). Considerably less is spectroscopically known about the intermolecular degrees of freedom, which are more directly sensitive to the angular-radial dependence (i.e., the global ''shape'') of the hydrogen bond potential. The relatively limited information on these low-frequency modes has made rigorous comparisons between experiment and theory significantly more difficult. As one example addressed in this work, spectroscopic information on these intermolecular modes is essential to include correctly zero-point contributions in any quantitative comparison of the equilibrium binding energy (D_e), which comes directly from *ab initio* calculations, with the dissociation energy (D_0) determined from experiment. It is worth noting that due to large amplitude motion of the light H atoms, the magnitude of this correction (i.e., the difference between D_0 and D_e) proves to be quite significant, more than 50% of D_0 itself.

There has been considerable theoretical effort[20–40] aimed at understanding the intermolecular forces in $(HF)_2$, with a major goal being to model and interpret the high-resolution experimental data. High level *ab initio* techniques have been used to calculate both the binding energy and equilibrium structure of the dimer. From these calculations, frequency estimates of the four intermolecular modes have been obtained using the harmonic force fields determined from the curvatures of the potential energy at the minimum energy configuration. However, due to large amplitude, anharmonic motion in the hydrogen bonded vibrational modes, such harmonic predictions provide only rough estimates of the true intermolecular vibrational frequencies. Alternatively, less sophisticated *ab initio* techniques have been used to calculate a sufficiently large number of potential energy points to permit an analytical multidimensional potential energy surface to be constructed. Two such potentials, which are analytical func-

[a]NIST-NRC postdoctoral fellow.
[b]Staff member, Quantum Physics Division, National Institute of Standards and Technology.

tions of all 6 internal degrees of freedom, are the *ab initio* surface of Bunker *et al.*[29,35] (BJKLK) and the semiempirical surface of Quack and Suhm (SQSBDE).[39] Both surfaces are based on the *ab initio* data of Kofranek *et al.*,[31] but the Quack and Suhm surface has been empirically adjusted to reproduce available experimental quantities such as the dissociation energy and ground state B rotational constant.

Though essential, the availability of a trial 6-D potential surface is only one step in the process; one also requires methods to solve accurately for the large amplitude quantum 6-D motion of the nuclei. This is an area which has been the focus of intense research effort:[39,41–49] recent developments in multidimensional quantum mechanics now allow solution of the corresponding full 6-D bound state eigenfunctions and eigenvalues for diatom–diatom systems such as HF dimer.[44,46,47] Thus fully converged predictions for the four intermolecular vibrational modes exist for both potentials listed above, which implicitly include all zero-point and anharmonic effects. This is particularly exciting, since such predictions of the intermolecular frequencies provide an essential link between experimental measurement and further refinement of the hydrogen bond potential surface. In addition, since the intermolecular vibrations sample portions of the multidimensional potential energy surface significantly different from the ground state, direct observation of these intermolecular modes offers a rigorous and independent test of the accuracy of such surfaces. As we shall see, even though quite reasonable agreement exists between theory and experiment for the dissociation energy (D_0) and equilibrium configuration of $(HF)_2$, considerable global errors still remain in these potentials, especially sampling at intermolecular vibrational geometries far from the equilibrium configuration.

The four zero-order intermolecular vibrational modes in $(HF)_2$ correspond to angular-radial motion predominantly in the van der Waals stretch (ν_4), in-plane geared (ν_5) and antigeared (ν_3) bends, and out-of-plane torsion (ν_6) of the two HF subunits. From previous experimental efforts in both the near[15,16] and far-ir,[5–8] the two lower intermolecular modes, the ''van der Waals stretch'' (ν_4) and ''geared bend'' (ν_5) are known to be at 125.1 and 160.6 cm^{-1}, respectively, while the out-of-plane torsion (ν_6, $K=1$) is significantly higher at 399.8 cm^{-1}. Prior to this study, the fourth and highest energy intermolecular mode, ν_3, had not been observed but was predicted from 6-D quantum calculations[44] to be around 425 cm^{-1}. Classically, this ν_3 vibration corresponds to an ''antigeared'' bend motion, i.e., frustrated in-plane internal rotation of the two HF monomers in the *same* direction. The relatively high frequency of this in-plane bending mode arises because motion along this coordinate quickly breaks the donor–acceptor hydrogen bond. For in-plane configurations of HF dimer, there also exists a much lower energy angular channel along the so-called ''geared'' bend coordinate, where the two HF monomers counter rotate in *opposite* directions. This lower energy path is largely responsible for the interconversion tunneling motion in $(HF)_2$, and results in the well-known splitting of the rovibrational levels evidenced in all $(HF)_2$ spectra. Thus, the antigeared and geared bend vibrations map out the *in-plane* portions of the potential surface responsible for tunneling phenomena. The corresponding torsional degree of freedom on the potential surface is predominantly sampled by the *out-of-plane* ν_6 torsional vibration, which corresponds to an azimuthal twisting of the subunits around the intermolecular axis defined by the two HF monomers center-of-mass axis.

One must be cautious when trying to assign descriptive quantum labels to these intermolecular vibrations. Specifically, for relatively weak restoring forces and highly anharmonic potentials, there can be considerable mixing between the different degrees of freedom that render such descriptive labels approximate. As one especially relevant case in point, the two nearly degenerate ν_4 and ν_5 modes, which correspond nominally to van der Waals stretch and geared bend excitation, have been shown[16] to be substantially mixed in $(HF)_2$. However, due to a combination of vibrational symmetry and energy separation, this is less likely to be the case among the two higher frequency ν_3 and ν_6 intermolecular modes. For example, the ν_6 mode is the lowest energy out-of-plane ($\Gamma_{vib}=A^-$) mode, and therefore can not vibrationally couple with any overtone or combination state of the in-plane ($\Gamma_{vib}=B^+/A^+$) vibrations. Conversely, although the antigeared bend mode is not prevented by symmetry from mixing with the other two in-plane intermolecular vibrational states, its relatively high vibrational frequency keeps it ''detuned'' from fundamentals and low order combination bands of the other even parity vibrational states.

Previous combination band studies in our laboratory of the intermolecular modes built on one quantum of high-frequency intramolecular excitation have demonstrated the unique advantages of the near-ir method.[16] Specifically, the use of near-ir laser light sources offers *continuous*, single mode tuning over spectral regions as large as several thousands of wave numbers. This makes possible extensive high-resolution searches for $(HF)_2$ combination spectra, and reliably establishes the relative integrated intensities of these bands. As an important corollary, this capability also allows us to indicate when bands are *not observed*, and therefore to quantify lower limits on the experimental band strengths. In addition, the use of a slit supersonic expansion source permits large concentrations of dimer species at low vibration/translation/rotational temperatures (10 K) and provides long direct absorption path lengths ideally suited for spectroscopic detection at high sensitivity. This combination of long path length, high cluster concentration, and near shot noise limited absorbance permits detection of combination bands more than 1000-fold weaker than the strongest intramolecular fundamentals, which has made possible observation of *all four* $(HF)_2$ intermolecular modes in the near-ir. Finally, since the near-ir excitation frequency exceeds the dissociation energy of the complex, vibrational predissociation in the upper state can and does occur. This opens new dynamical channels not accessible in the far-ir, the rates of which can be obtained from high-resolution measurements of the homogeneous broadening for individual rovibrational transitions.

In the present study, the ''high'' energy intermolecular

modes ν_3 and ν_6 are observed in combination with the ν_1 and ν_2 HF-stretch intramolecular vibrations, respectively. In conjunction with the well-established intramolecular fundamental data,[6,9,10,13] this permits accurate measurement of both the intermolecular frequencies and tunneling splittings in the HF-stretch excited state manifold. Furthermore, linewidth measurements permit the dependence of HF-stretch-induced vibrational predissociation lifetimes on intermolecular excitation to be elucidated. The linewidths measured for these combination states predominantly reflect a dependence on intramolecular mode, but also show a dependence on the intermolecular vibration consistent with trends first identified for the lower energy ''van der Waals stretch'' and ''geared bend'' combination bands. Reliable extrapolation to the corresponding ν_3 and ν_6 intermolecular fundamentals is possible based on the current near-ir measurements of the $\nu_1+\nu_3$ and $\nu_2+\nu_6$ combination bands. The predicted frequencies for ν_6 are in reasonable agreement with 6-D quantum calculations, but the ν_3 value is considerably *underestimated* indicating that further refinement of the current $(HF)_2$ potentials is necessary. This discrepancy also has important implications for intermolecular zero-point energy contributions to the dissociation energy, which are necessary to obtain an experimentally based estimate of the binding energy (D_e).

The remainder of this paper is organized as follows: In Sec. II we briefly describe the experimental apparatus and experimental conditions used to form and detect $(HF)_2$. In Sec. III the data and the assignments (intramolecular, intermolecular, and tunneling state) are presented for the ν_6 and ν_3 combination bands, along with a brief spectroscopic analysis. In Sec. IV, the tunneling splittings and predissociation lifetimes measured for the intermolecular excited states are analyzed in detail. Furthermore, extrapolation procedures to obtain the best experimental estimates of the intermolecular fundamental frequencies are compared with 6-D quantum calculations on trial potential surfaces. Finally, an experimentally based estimate for D_e is determined using the ν_1 and ν_2 redshifts, D_0 and intermolecular zero-point energies based on measurements of all four intermolecular modes. Section V summarizes our conclusions and describes directions for future work.

II. EXPERIMENT

The experimental technique employed in this project is identical to that used in previous[16] studies of $(HF)_2$ and is described in detail elsewhere.[50,51] Briefly, the combination band spectra of $(HF)_2$ are recorded using a slit supersonic jet for low temperature (8–10 K) cluster formation and direct infrared absorption methods based on a tunable, narrow band (1–2 MHz) difference frequency spectrometer. Clusters of HF are produced in the supersonic expansion using a mixture of 1% HF in a 50–50 mix of Ar and Ne-70, typically at backing pressures of 450 Torr. These conditions have been empirically determined to optimize the formation of $(HF)_2$, although as reported earlier,[16,52] for the weaker combination bands $(\nu_1+\nu_3)$ small amounts of N_2O are added to the mix $(\sim 1\%)$ to enhance the $(HF)_2$ signals by up to 50%. The laser

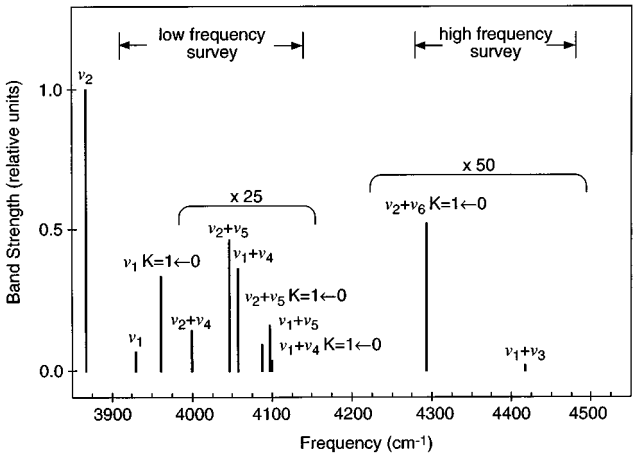

FIG. 1. Overview of the near-ir fundamental and combination band spectrum of $(HF)_2$ in a slit jet ($K=0\leftarrow 0$ unless otherwise specified). Indicated in the figure are the two spectral regions surveyed for combination bands, a ''low'' frequency region from 3850–4200 cm^{-1} and a ''high'' frequency region from 4280–4480 cm^{-1}. The transition strengths of the combination bands have been multiplied by 25 and 50 in order to plot the combination bands on the same scale as the intramolecular fundamentals. For visual clarity only one of the tunneling components are shown for each fundamental and combination band.

frequency stability and high signal-to-noise (S/N) of the spectra permit measurement of relative frequencies to a precision better than 0.0002 cm^{-1}, as verified by the routine agreement with microwave combination differences at the 5 MHz level. Absolute frequency calibration of the $\nu_2+\nu_6$ combination band ($\sim$4290 cm^{-1}) is made with respect to the $R(0)$ transition [4263.837 196(5) cm^{-1}] of the first overtone[53] of CO. Similarly, the $\nu_1+\nu_3$ combination band ($\sim$4418 cm^{-1}) is referenced to the $R(3)$ transition [4420.6480(2) cm^{-1}] of the first overtone[54] of the antisymmetric stretch of N_2O. This calibration procedure allows the transition frequencies and vibrational origins to be reported to an absolute accuracy of 0.0004 cm^{-1}.

III. RESULTS AND ANALYSIS

Based on previous far-ir experimental data[5] and predictions of the intermolecular mode frequencies,[44] the search for HF dimer combination bands associated with the two ''high'' frequency intermolecular modes (ν_3 and ν_6) is performed over the 200 cm^{-1} region between 4280 and 4480 cm^{-1}. An exhaustive search over this region reveals only four vibration–rotation–tunneling (VRT) bands; these bands reflect excitation in each of the ν_3 and ν_6 intermolecular modes, built on either the ν_1 or ν_2 intramolecular fundamentals. A stick spectrum that schematically summarizes the vibrational origins and relative integrated intensities for the combination bands reported in this paper is shown in Fig. 1, along with similar data on the ''low'' frequency ν_4 and ν_5 combination bands observed previously.[16] Note that the $\nu_2+\nu_6$ combination band is relatively strong, i.e., down by only 95-fold from the ν_2 $K=0\leftarrow 0$ fundamental band $(K=K_a)$. However, the $\nu_1+\nu_3$ combination band is the weakest observed in $(HF)_2$, down in intensity by nearly a factor of 2500 from the ν_2 fundamental.

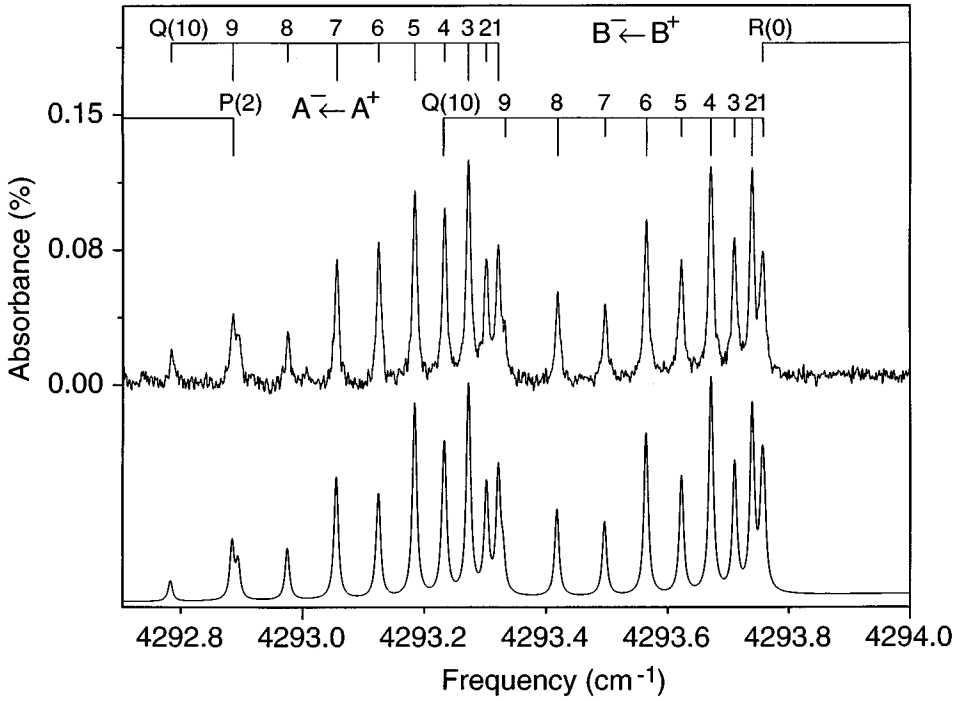

FIG. 2. A section of the spectrum near the origin of the $K=1\leftarrow0$ subband of the $\nu_2+\nu_6$ combination band of $(HF)_2$. The A^+ and B^+ symmetry labels refer to $\Gamma_{\text{vib-tun}}$, the vibration–tunneling symmetry. The simulated spectrum at the bottom of the figure is generated using the fitted rotational constants, a $T_{\text{rot}}=10(1)$ K rotational temperature, and a J-independent predissociation broadening of 250(20) MHz (see the text for details).

A. Out-of-plane torsion (ν_6)

($\nu_2+\nu_6$) $K=1\leftarrow0$

Based on the low rotational temperatures achieved in the slit jet expansion and the symmetry requirements[55–59] for dipole mediated transitions in $(HF)_2$, perpendicular $K=1\leftarrow0$ transitions are anticipated to be strongest for combination bands with one quantum of ν_6 excitation. The two possible near-ir frequencies for these $K=1\leftarrow0$ bands can be crudely estimated by adding the frequency of the $(K=1\leftarrow0)$ out-of-plane torsion fundamental measured in the far-ir[5] to either the ν_1 or ν_2 fundamental frequency.[10] Furthermore, due to stronger hydrogen bonding in the intramolecular *excited* state which tends to increase the intermolecular frequencies, the combination bands should be somewhat blueshifted from these predictions. Qualitatively consistent with these expectations, a strong $K=1\leftarrow0$ subband of $(HF)_2$ is observed at 4293 cm^{-1} (approximately 100-fold weaker than the ν_2 $K=0\leftarrow0$ fundamental), which is close to but at a higher energy than the 400 $cm^{-1}+3868$ $cm^{-1}=4268$ cm^{-1} origin one estimates for the $\nu_2+\nu_6$ band. Conversely, the $\nu_1+\nu_6$ band origin would be predicted at 4331 cm^{-1}, which is already higher than observed experimentally. Shown in Fig. 2 is a section of the spectrum containing the Q-branch region for the two VRT bands, one for each tunneling level. Lower state combination differences calculated using the corresponding R- and P-branch transitions ($\sigma_{\text{rms}}=0.0005$ cm^{-1}) indicate unambiguously that these transitions arise from the $K=0$ state of HF dimer.

In addition, these combination differences can be used to assign the ground state tunneling symmetry for each VRT band, which are further verified by the intensity alternation apparent in Fig. 2. Specifically, due to nuclear spin statistics, the intensities in even:odd J'' are 10:6(6:10) for transitions originating from the $\Gamma_{\text{vib-tun}}=A^+(B^+)$ level of the $K=0$ ground state, respectively. Symmetry assignments refer to the irreducible representations in the MS_4 molecular symmetry group as discussed in more detail elsewhere.[16,57] All transitions from $R(9)$ through $P(5)$, including $Q(1)-Q(9)$, are observed for each VRT band and reported in Table I. The rotational progressions for each VRT band are fit separately to

$$E_K(J)=\nu_K+[\overline{B_K}\pm 1/4 b_K\delta_{K1}]J(J+1)-D_K J^2(J+1)^2 + H_K J^3(J+1)^3. \quad (1)$$

In Eq. (1), ν_K is defined as the energy of the $J=0$ (extrapolated for $K>0$) state for a given K level. In addition, B_K, D_K, and H_K are the K-dependent effective rotational and distortion constants in symmetric top notation, while the Kronecker delta δ_{K1} brings in an asymmetry splitting term $(b_K=(B_K-C_K))$ which is only significant for $K=1$ levels. For the spectra presented in this paper, the ground state constants are held fixed at values previously determined from global fits to both microwave and near-ir data.[8,17,60] Furthermore, upper state sextic centrifugal distortion constants, H_K, are set to zero due to the lack of high J transitions necessary for an accurate determination. The results of the fits to Eq. (1) are summarized in Table II. A comparison of the experimental data with a simulated spectrum generated using a sum of Voigt line shapes and the constants reported in Table II is also shown in Fig. 2. Excellent agreement between experi-

TABLE I. Transition frequencies (in cm^{-1}) for the $\nu_2+\nu_6$ $K=1\leftarrow0$ and $\nu_1+\nu_3$ $K=0\leftarrow0$ VRT bands in $(HF)_2$. The $A^{\pm}B^{\pm}$ symmetry labels refer to $\Gamma_{\text{vib-tun}}$. Numbers in parentheses represent (observed–calculated) values based on the fitted constants listed in Table II.

	$\nu_2+\nu_6$ $K=1\leftarrow0$		$\nu_1+\nu_3$ $K=0\leftarrow0$	
	$A^-\leftarrow A^+$	$B^-\leftarrow B^+$	$B^+\leftarrow A^+$	$A^+\leftarrow B^+$
$R(8)$	4297.2669(−3)		4421.1431(−1)	4420.6078(−1)
$R(7)$	4296.9158(3)	4296.4647(0)	4420.8459(4)	4420.3137(2)
$R(6)$	4296.5546(3)	4296.1058(−6)	4420.5328(3)	4420.0042(3)
$R(5)$	4296.1834(−3)	4295.7386(3)	4420.2042(−1)	4419.6792(4)
$R(4)$	4295.8036(−2)	4295.3604(0)	f	4419.3388(4)
$R(3)$	4295.4143(−4)	4294.9733(4)	4419.5022(−2)	4418.9828(3)
$R(2)$	4295.0163(−3)	4294.5764(4)	4419.1291(2)	4418.6114(3)
$R(1)$	4294.6091(−5)	4294.1699(−1)	4418.7404(0)	4418.2246(3)
$R(0)$	4494.1936(0)	a	4418.3371(3)	4417.8219(−1)
$Q(1)$	4293.7574(−19)[b]	4293.3206(−2)		
$Q(2)$	4293.7397(−2)	4293.3011(−2)		
$Q(3)$	4293.7105(−4)	4293.2717(−2)		
$Q(4)$	4293.6715(−6)	4293.2324(−2)		
$Q(5)$	4293.6231(−4)	4293.1832(−1)		
$Q(6)$	4293.5655(4)	4293.1236(−2)		
$Q(7)$	4293.4974(7)	4293.0543(2)		
$Q(8)$	4293.4180(−3)	4292.9739(−1)		
$Q(9)$	c	4292.8842(10)[d]		
$Q(10)$		4292.7818(1)		
$P(1)$			4417.4844(−5)	4416.9714(3)
$P(2)$	4292.8941(6)[e]	4292.4573(18)	4417.0369(3)	4416.5222(−4)
$P(3)$	4292.4438(11)	4292.0043(−2)	4416.5739(3)	4416.0589(1)
$P(4)$	4291.9834(0)	4291.5451(4)	4416.0950(1)	4415.5796(−2)
$P(5)$	4291.5163(8)	4291.0763(2)	4415.6032(0)	4415.0853(−4)
$P(6)$	4291.0388(−1)		4415.0961(1)	4414.5759(−6)
$P(7)$			4414.5759(16)[g]	4414.0522(−2)
$P(8)$			4414.0380(−1)	4413.5130(−6)
$P(9)$			4413.4872(−3)	

[a]Overlap with $Q(1)$ of $A^-\leftarrow A^+$.
[b]Overlap with $R(0)$ of $B^-\leftarrow B^+$.
[c]Overlap with $Q(1)$ of $B^-\leftarrow B^+$.
[d]Overlap with $P(2)$ of $A^-\leftarrow A^+$.
[e]Overlap with $Q(9)$ of $B^-\leftarrow B^+$.
[f]Overlap with $R(3)$ of N_2O.
[g]Overlap with $P(3)$ of N_2O.

ment and the simulated spectrum, both in frequency and relative intensities, is achieved for a slit jet temperature of 10(1) K and a J-independent vibrational predissociation broadening of 250(20) MHz.

The ν_2 *intramolecular* assignment of this band is first suggested by the much better agreement between predicted and observed vibrational origins for $\nu_2+\nu_6$ vs $\nu_1+\nu_6$ excitation and, as described below, also confirmed by a combination of linewidth and tunneling symmetry arguments. From a high-resolution linewidth analysis discussed in Sec. V, the transition profiles are dominated by 250(20) MHz contributions from predissociation broadening. This is comparable to than the 330 MHz predissociation linewidth measured[13] for ν_2 and yet >20-fold larger than the 6–12 MHz values observed in ν_1. Based on the relatively weak intermolecular mode dependence of vibrational predissociation observed in our previous studies[16] of ν_4 and ν_5, this strongly indicates a combination band built on ν_2. Additional corroboration of the ν_2 intramolecular assignment is obtained from the energy ordering of the tunneling levels in the upper vibrational state. Based on an intermolecular assignment to the out-of-plane torsion, the relative ordering of the two VRT bands is consistent with $\Gamma_{\text{vib}}=\Gamma_{\text{intra}}\otimes\Gamma_{\text{inter}}=A^-$, and thus a ν_2 ($\Gamma_{\text{intra}}=A^+$) intramolecular mode assignment. Specifically, this assignment implies an A^+/B^+ ordering of tunneling symmetry levels in the $\nu_2+\nu_6$ state and thus a *positive* tunneling splitting as defined in Ref. 17. Indeed, in all 14 VRT bands observed in combination with the ν_1/ν_2 dyad in HF dimer, we have found no exception to this pattern, i.e., all vibrational assignments indicate the $\Gamma_{\text{tun}}=A^+$ tunneling level to be the lower energy state in each tunneling pair.

As a test of internal consistency, the sign of the asymmetry splitting leads to the identification of these VRT bands as C-type, and thus that the vibrational parity of the upper state is commensurate with the out-of-plane torsion ν_6 *intermolecular* vibrational assignment. The resulting intermolecular vibrational energy is obtained by subtracting the ν_2 fundamental [3868.0793(2) cm^{-1}] from the energy of the (lower) $\Gamma_{\text{tun}}=A^+$ state, yielding an intermolecular energy of 425.6897(5) cm^{-1} for the $K=1$ state of the out-of-plane torsion. As anticipated, there is an appreciable increase (+6.5%) in the ν_6 intermolecular frequency measured in the ν_2 excited state relative to the far-ir ν_6 measurement [399.787(1) cm^{-1}], consistent with a ''stiffening'' of the hydrogen bond in the HF-stretch excited states. In order to isolate the effect of ν_6 excitation on vibrationally averaged geometries in both the ground and ν_2 excited states, the

TABLE II. Molecular constants (in cm^{-1}) from spectral fits of the combination bands assigned to the (ν_6) out-of-plane torsion and (ν_3) antigeared bend. All origins are reported with respect to the $\Gamma_{VRT}=A^+K=0$ ground vibrational state of $(HF)_2$. The uncertainties in parentheses represent 2σ in the units of the last reported digit.

	$\nu_2+\nu_6$, $K=1$		$\nu_1+\nu_3$, $K=0$	
$\Gamma_{\text{vib-tun}}$	A^-	B^-	B^+	A^+
ν_0	4293.7690(5)	4293.9893(3)	4417.9183(3)	4418.0629(3)
B	0.212 117(32)	0.211 900(16)	0.209 26(2)	0.208 87(2)
$D_K/10^{-6}$	2.58(40)	3.03(16)	1.96(26)	1.48(6)
$b_K/10^{-3}$	0.949(26)	0.825(15)	...[a]	...[a]
σ_{rms}	0.000 53	0.000 30	0.000 34	0.000 37

[a]There are no splittings for $K=0$.

changes in rotational $\bar{B}$ and D constants are calculated with respect to the corresponding state without ν_6 excitation. The changes in these constants upon ν_6 excitation are remarkably similar in the far- and near-ir. In both cases the B rotational constant decreases by approximately 3%, corresponding roughly to a 1.5% increase in the hydrogen bond length $(B \propto \langle 1/R^2 \rangle)$. Consistent with this elongation of the hydrogen bond, the D distortion constants increase in the ν_6 excited state, indicating a reduced hydrogen bond restoring force. One simple physical interpretation of this rotational analysis is that *nonplanar* configurations lead systematically to a *weaker*, and therefore, *longer* hydrogen bond. This also provides corroborating evidence for relatively weak coupling between inter- and intramolecular degrees of freedom, i.e., while ν_2 excitation increases the ν_6 intermolecular energy, it does not dramatically influence the intermolecular character of the ν_6 vibration.

For $\nu_2+\nu_6$ excitation ($\Gamma_{vib}=A^-$), the *difference* in the two VRT band origins equals the *increase* in the tunneling splitting between the lower and upper vibrational state. The tunneling splitting in the upper state is therefore determined to be 0.2203(6) cm^{-1}, which is 50% smaller than the tunneling splitting in the ν_2 $K=1$ state [$\Delta\nu_{tun}=0.3411(9)$ cm^{-1}]. This relatively small change in the tunneling splitting in the ν_6 intermolecular excited state is roughly consistent with far-ir measurements, where the tunneling splitting increases slightly from 1.064 437 4(1) cm^{-1} in the $K=1$ ground state to 1.626(1) cm^{-1} in the ν_6 $K=1$ excited state. Thus unlike the more dramatic 8–15-fold increases in tunneling splitting measured for both ν_4 and ν_5 excitation,[16] this ''high'' energy intermolecular mode appears to have only a relatively modest effect on the interconversion tunneling splitting. We return to a more detailed analysis of the intermolecular mode specific tunneling dynamics in the discussion section.

As one final point, the analogous combination band built on the ''free'' HF-stretch (i.e., the $K=1\leftarrow0$ band of $\nu_1+\nu_6$) is *not* experimentally observed. Given the transition strength and S/N of the $\nu_2+\nu_6$ $K=1\leftarrow0$ combination band, the corresponding band built on ν_1 should be easily detectable. Furthermore, the anticipated blueshift of $\nu_1+\nu_6$ from the $\nu_2+\nu_6$ origin can be readily estimated from the differential ν_1 and ν_2 fundamental shifts to within a few cm^{-1} uncertainty; thus spectral search is not an issue. From previous work with the lower energy ν_4 and ν_5 $(HF)_2$ combination bands, the $\nu_1+\nu_6$ combination band transitions would be anticipated to be as much as an order of magnitude *narrower* than in the $\nu_2+\nu_6$ combination band; this should make detection using high-resolution spectroscopy even easier since the same integrated band strength is concentrated into sharper lines. Despite these experimental advantages, however, we have not been able to observe the $\nu_1+\nu_6$ $K=1\leftarrow0$ combination band. Based on S/N and linewidth considerations this indicates that the $\nu_1+\nu_6$ band must be down at least a factor of 200 in transition strength from the corresponding $\nu_2+\nu_6$ band. This is one of several examples of anomalous intensity effects seen in both the HF and DF dimer combination band spectra, and which thus far are *not even qualitatively* explained by full 6-D calculations on trial potential surfaces.

B. Antigeared bend (ν_3)

($\nu_1+\nu_3$) $K=0\leftarrow0$

Prior to the present study, the antigeared bend (ν_3) in $(HF)_2$ had not been observed either in the far-ir or via combination bands in the near-ir, though full 6-D quantum calculations[44] on the best available potential surfaces predicted it to be around 425 cm^{-1}. Initial search efforts to observe $\nu_1+\nu_3$ in our laboratory were guided by these numbers, centered around 3931 cm^{-1}+425 cm^{-1}=4360 cm^{-1}. Despite comprehensive single mode scans, no bands due to $(HF)_2$ are evident in a 50 cm^{-1} window around this region. However, approximately 60 cm^{-1} *further to the blue* of the original estimate, two weak overlapping bands (~0.1% the integrated intensity of the $K=0\leftarrow0$ ν_1 fundamental) are observed around 4418 cm^{-1}; a section of the spectrum is shown in Fig. 3. The simple P/R-branch structure for each VRT band, the presence of $R(0)$ and $P(1)$, and the approximately $4B\approx0.8$ cm^{-1} ''null gap'' confirm that each VRT band is a $K=0\leftarrow0$ band of $(HF)_2$. Ground state combination differences ($\sigma_{rms}=0.0004$ cm^{-1}) allow for unambiguous J'' labeling of the transitions, as well as the $\Gamma_{vib\text{-}tun}$ symmetry in the lower state. The symmetry assignments determined from combination differences are verified by intensity alternation in J present in the spectrum (see Fig. 3). All transitions from $R(8)$ to $P(8)$, inclusive, are observed for each of the two VRT bands and are reported in Table I. The molecular constants obtained by fitting the rotational progressions to Eq. (1) are summarized in Table II. Included in Fig. 3 is a simulated spectrum based on the fitted molecular constants and a 10 K slit jet temperature.

The relatively narrow predissociation linewidths measured for the individual rovibrational transitions [90(20) and 60(20) MHz for the $A^+\leftarrow B^+$ and $B^+\leftarrow A^+$ VRT bands, respectively] suggest a ν_1 intramolecular assignment, though these are substantially broadened beyond the values for the pure ν_1 fundamental. This ν_1 assignment is additionally confirmed by the relative origins of the two VRT bands and the expectation of positive tunneling in the upper state.[17] Specifically, the $\Gamma_{vib\text{-}tun}=A^+\leftarrow B^+$ origin is at higher frequency than the $\Gamma_{vib\text{-}tun}=B^+\leftarrow A^+$ origin, which means a $\Gamma_{vib\text{-}tun}=B^+(A^+)$ symmetry for the lower (upper) tunneling level in the upper vibrational state. Thus for the lower energy tunneling level to have $\Gamma_{tun}=A^+$ symmetry requires $\Gamma_{vib}=\Gamma_{intra}\otimes\Gamma_{inter}=B^+$, which for any in-plane intermolecular mode ($\Gamma_{inter}=A^+$) implies the corresponding intramolecular vibration must be ν_1 ($\Gamma_{intra}=B^+$). The intermolecular frequency is determined by subtracting the ν_1 fundamental [3930.9030(2) cm^{-1}] from the origin of the $B^+\leftarrow A^+$ VRT band, which yields 487.0153(4) cm^{-1}.

As this 487 cm^{-1} intermolecular mode is now almost 1/2 the dissociation energy of HF dimer, the assignment of this intermolecular component to the ν_3 antigeared bend requires more subtle consideration. Unlike the out-of-plane torsion, symmetry arguments alone are not sufficient; any of the three in-plane intermolecular vibrations (all $\Gamma_{inter}=A^+$) or combinations thereof could conceivably give rise to this combination band. Thus, even though ν_3 is the only *fundamental*

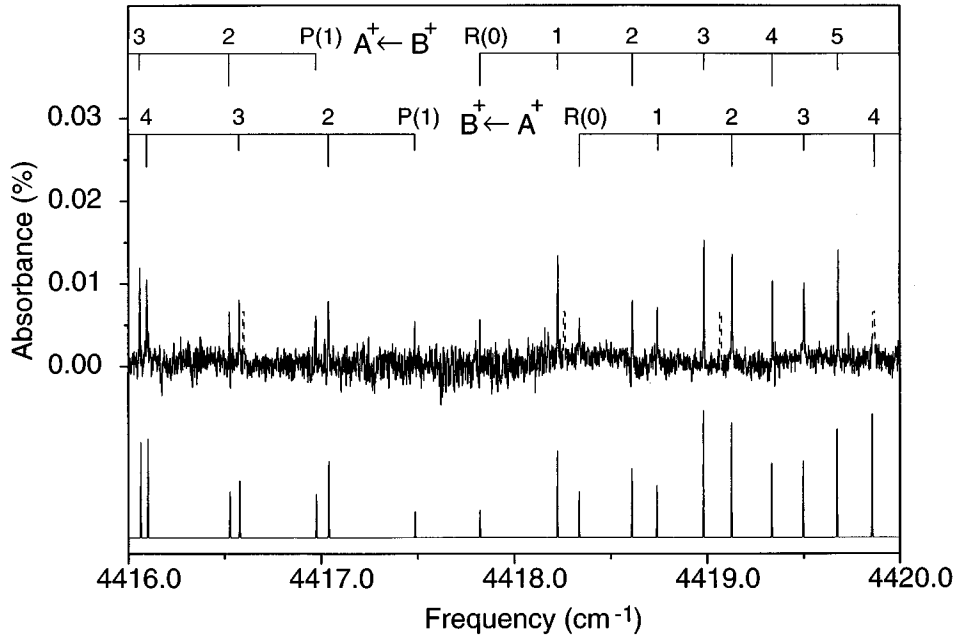

FIG. 3. Spectral region near the origins of the two $K=0\leftarrow 0$ VRT bands of the $\nu_1+\nu_3$ combination band of $(HF)_2$. The simulated spectrum at the bottom of the figure was calculated using the fitted rotational constants and a 10 K rotational temperature. Additional peaks due to the $(20^00)\leftarrow(00^00)$ rovibrational transitions of monomeric N_2O, added to increase the $(HF)_2$ signal (see the text), are truncated and dashed to emphasis the $(HF)_2$ spectrum.

vibration of the correct $\Gamma_{\text{inter}}=A^+$ symmetry predicted within 300 cm^{-1}, *multiply* excited ν_4 and ν_5 states are in principle accessible at this high an intermolecular energy.

Our assignment of this band to $\nu_1+\nu_3$ excitation is based on the following experimental data. First of all, any assignment not involving ν_3 would require at least *three* quanta of intermolecular excitation distributed between the low-frequency ν_4 and ν_5 intermolecular modes. Given the 25-fold reduction in the integrated intensity between the *strongest* binary combination band and intramolecular fundamental, one would anticipate such exotic combination bands with four quanta of inter/intramolecular excitation to be an additional several orders of magnitude weaker than experimentally observed. Indeed, quantum calculations of far-ir transitions strengths[61] support such a rapid drop off in intensity for the intermolecular overtones and combination bands. Secondly, both the ν_4 and ν_5 intermolecular modes have been found experimentally to increase the tunneling splitting in both the ν_1 and ν_2 excited states by 8–15-fold; thus any assignment that included *multiple* quanta in these two modes would be expected to exhibit an anomalously *large* tunneling splitting. By way of contrast, the tunneling splitting in the upper state is 0.1447(4) cm^{-1}, which is comparable and even a bit *smaller* than the corresponding 0.2155(3) cm^{-1} splitting in ν_1. Third, continuous single mode spectral scans 80 cm^{-1} both to the red and blue of this band confirm this as the *only* state with sufficient oscillator strength for us to detect with the slit jet spectrometer. This 160 cm^{-1} region is certainly a sufficiently broad window to include the $\nu_1+\nu_3$ combination band. Thus even though other (e.g., $\nu_1+3\nu_5$, $\nu_1+3\nu_4$, $\nu_1+\nu_4+2\nu_5$, $\nu_2+3\nu_5$, etc.) combination bands are also predicted to be in the region surveyed, it seems a highly unlikely scenario that $\nu_1+\nu_3$ would *not* be observable while one (and only one) of these higher order combination bands would be detected. As a final confirmation, analogous single mode spectral scans for all four intermolecular modes in DF dimer also reveal only one ''bright'' state at intermolecular energies higher than the out-of-plane torsion, which we have assigned[62] as the corresponding $\nu_1+\nu_3$ combination band in $(DF)_2$.

As discussed previously,[16] pure descriptive labels for these intermolecular states can be difficult to make unambiguously. Since ν_3 has $\Gamma_{\text{inter}}=A^+$ vibrational symmetry, it can in principle be mixed with any overtone/combination states of both van der Waals stretch and geared bend character. Indeed, the 4% decrease in the B rotational constant between $\nu_1+\nu_3$ and ν_1 may already indicate partial van der Waals stretch character in the ν_3 intermolecular state due to radial-angular coupling along the anti-geared bending coordinate. Such an interpretation is qualitatively corroborated by analysis of eigenfunction nodal patterns from full 6-D quantum calculations.[44] However, since this is the only ''bright'' combination state experimentally observed within ± 80 cm^{-1} of the $(HF)_2$ frequency region anticipated for ν_3, this intermolecular state is likely to have predominantly anti-geared bend character. A more descriptive intermolecular mode assignment will be discussed in the comparison with theory.

IV. DISCUSSION

A. Donor–acceptor interchange tunneling

In a molecule such as $(HF)_2$ that has four intermolecular degrees of freedom and only one low energy tunneling coordinate (corresponding approximately to a ''geared'' rotation

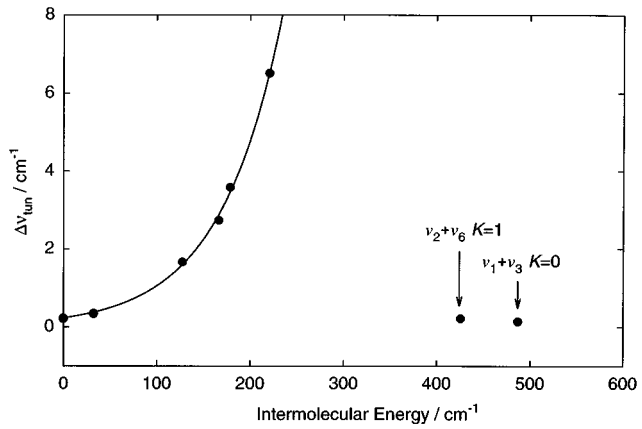

FIG. 4. Plot of the upper vibrational state tunneling splitting versus intermolecular energy for all the $(HF)_2$ combination bands observed to date. The ''low'' energy ν_4 and ν_5 intermolecular excited states display a dramatic increase in the observed tunneling splitting while the ''high'' energy ν_3 and ν_6 intermolecular excited states do not. This is one of several indications that both ν_3 and ν_6 correlate only very weakly with the tunneling coordinate in $(HF)_2$. The solid curve is from a WKB analysis of the two low frequency ν_4, ν_5 intermolecular modes in Ref. 16.

of the HF subunits), intermolecular excitation might be expected to increase the donor–acceptor tunneling rate in a strongly mode specific fashion. Due to spectral congestion in cooled cell far-ir studies,[5–8] however, there has been little data available for the tunneling splittings in intermolecular excited states with which to test such predictions. For example, the only previous far-ir direct experimental observation[5] of a tunneling splitting for an intermolecular excited state is for ν_6 $(K=1)$. Supersonic jet combination band data in the near-ir,[15,16] now provides a significantly larger body of information on the intermolecular mode specificity of the tunneling splitting in HF-stretch excited states than available in the ground HF-stretching states. In interpreting these data, one must take into account both *intra-* and *inter*molecular contributions to the observed tunneling splitting in near-ir combination states, which makes isolating the intermolecular dependence more difficult. Indeed, considerable theoretical effort[10,35,39,45,58,60,63–67] has centered on the correct dynamical interpretation for the threefold reduction in the tunneling splitting between the ground and H(D)F-stretch excited states (ν_1 and ν_2) in both HF and DF dimer. To a reasonable level of approximation, however, the intermolecular dependence can be isolated by comparing *ratios* of the tunneling splitting for a combination state (i.e., $\nu_1/\nu_2+\nu_{\text{intermolecular}}$) with the corresponding ν_1/ν_2 fundamental state.

Previous combination band studies[15,16] of the ''low frequency'' (<200 cm^{-1}) intermolecular modes in $(HF)_2$ have shown that both ν_4 and ν_5 excitation greatly increase (approximately 8–15-fold) the tunneling splitting in HF-stretch excited states. These two low frequency degrees of freedom appear to be strongly mixed in HF dimer, with both ν_4 and ν_5 having appreciable ''geared bend'' character. This appears not to be true for the modes in DF dimer,[62] and thus must be a function not only of coupling in the potential but also vibrational near resonances. As a consequence, the tunneling rates in HF dimer for these two low frequency vibrations are relatively mode-insensitive, and instead depend predominantly on the *total* intermolecular energy and the barrier to interconversion. As described previously,[16] the energy dependence of the tunneling rates for ν_4 and ν_5 can be remarkably well characterized by a simple 1-D tunneling model and a WKB analysis of the tunneling splittings (see Fig. 4).

In sharp contrast to these results for the low frequency intermolecular modes, both ν_6 and ν_3 excitation do not influence the tunneling splitting significantly. This behavior is demonstrated in Fig. 4, where all the tunneling splittings measured in HF-stretch excited states are plotted as a function of intermolecular energy; the relevant values are also summarized in Table III. The tunneling splittings measured for both ν_3 and ν_6 obviously do not follow the simple WKB extrapolations for the ν_4 and ν_5 modes. This data suggests that the vibrational motion associated with these high frequency ν_3 and ν_6 modes has very little projection along the most effective tunneling pathway. Alternatively, the small tunneling splittings for ν_3 and ν_6 provide particularly strong evidence that the tunneling flux occurs primarily through the low energy ''geared'' transition state of the PES, rather than

TABLE III. Experimental and theoretical tunneling splittings (in cm^{-1}) of $(HF)_2$ in excited intermolecular states in the ground, ν_1 and ν_2 HF-stretching manifolds for both $K=0,1$.

		Ground state		ν_1		ν_2	
Vib.	K	Experiment	Theory[a]	Experiment	Theory[b]	Experiment	Theory[b]
g.s.	0	0.658 690(1)[c]	0.44	0.2155(3)[d]	0.128	0.2334(4)[d]	0.089
g.s.	1	1.064 437(1)[c]	0.86	0.3499(1)[d]		0.3411(9)[d]	
ν_3	0		15.02	0.1447(4)			
ν_4	0		0.98	1.6639(22)	0.796		0.410
ν_5	0		7.48	2.7391(11)	2.283	3.5868(9)	2.028
ν_5	1		18.65			6.5153(13)	
ν_6	0		1.75				
ν_6	1	1.626(1)				0.2203(6)	

[a]References 43, 44.
[b]Reference 45.
[c]References 8, 60.
[d]Reference 10.

over some linear combination of geared, antigeared, and out-of-plane barriers.

The strong *inter*molecular mode specificity of the tunneling splitting observed in $(HF)_2$ in the HF-stretch excited states is clearly the predominant effect, yet there is also evidence for a more subtle additional dependence on *intra*molecular excitation as well. For example, ν_6 excitation ($K=1$) in the ground HF-stretching state *increases* the tunneling splitting approximately 1.5-fold, while in the ν_2 excited state, ν_6 excitation ($K=1$) *decreases* the tunneling splitting by nearly the same factor. A simple physical model for such an effect could arise from intermolecular $V \rightarrow V$ transfer between the vibrationally excited tunneling subunits, which if mediated by near resonant electrostatic (e.g., dipole–dipole) interactions, would be slowed by the presence of a node in the planar configuration for ν_6 out-of-plane excitation. In any event, the experimental observations clearly indicate that while the intermolecular dependence can be *approximately* isolated by comparing the tunneling splittings in combination states with the corresponding ν_1/ν_2 states, this separation is *not* rigorous and the quantitative tunneling dynamics depend on all 6 internal degrees of freedom. Further evidence of a coupled inter/intramolecular dependence to the tunneling rates is also found in corresponding spectroscopic studies of the combination states of $(DF)_2$ as reported in detail elsewhere.[62]

The tunneling splittings in combination states provide a stringent test of the intra–intermolecular dependence of the full 6-D potential surface, particularly in the region of the barrier to interconversion. Quantitative predictions for tunneling splittings in states that include at least one quantum of HF-stretch excitation are computationally demanding, since it requires accurate quantum calculations of vibrationally metastable ''resonance states'' at energies substantially above the dissociation limit. Nevertheless, Zhang and co-workers[45] have recently succeeded in performing full 6-D quantum resonance calculations of the energy levels in HF-stretch excited states of $(HF)_2$, based on the SQSBDE potential of Quack and Suhm.[39] The results, shown in Table III, indicate that many of the tunneling splitting trends in HF-stretch excited states are qualitatively reproduced, but the calculated tunneling splittings consistently underpredict (by 15%–60%) the corresponding experimental values. Furthermore, the predicted tunneling splittings in the ν_1 excited states are systematically *larger* than the analogous levels in the ν_2 manifold, contrary to experimental findings (see Table III). At least for the two low frequency intermolecular modes, ν_4 and ν_5, the intermolecular dependence of the tunneling splitting in $(HF)_2$ is qualitatively well reproduced. This may be partially fortuitous, however, since the SQSBDE surface does not appear to correctly reproduce the strength of stretch-bend coupling experimentally observed in $(HF)_2$.[16]

An even more significant discrepancy between experiment and theory exists for the tunneling splitting in the ν_3 antigeared bend state. Analogous 6-D bound state calculations[44] for the ground HF-stretching states (Table III), predict a 34-fold *increase* in the tunneling splitting in the ν_3 antigeared bend fundamental state. This is dramatically different, both in magnitude and direction, from the 1.5-fold *decrease* observed between $\nu_1+\nu_3$ and ν_1. This would suggest that the strong enhancement in the tunneling rate predicted by quantum calculations for ν_3 is incorrect and results from inaccuracies in the PES's along the antigeared bend coordinate. This interpretation is further supported by disagreement between experimental and predicted ν_3 intermolecular frequencies, discussed in more detail later in Sec. IV C.

B. Vibrational predissociation

Previous studies of the geared bend and van der Waals stretch modes indicate that the predissociation rates from combination band excited states are dominated by the *intramolecular* mode, with a much weaker dependence on *intermolecular* mode.[16] Indeed, due to the large difference in the predissociation broadening for ν_2 (330 MHz) and ν_1 (6–12 MHz), this intuition proves useful in confirming assignments of the intramolecular component of combination bands. The two combination bands probed in this study have nearly 500 cm^{-1} of initial intermolecular excitation, which reflects at least 2-fold more intermolecular energy than any of the previous low frequency combination bands observed, and allows one to sample the intermolecular mode dependence of the predissociation rate at considerably higher energies.

The predissociation lifetimes are determined from a Voigt deconvolution of the HF dimer VRT linewidths.[16] The resulting Lorentzian component from such an analysis can be ascribed completely to predissociation broadening ($\Delta\nu_{pd}$), since the factors such as pressure and power broadening are negligible for the greatly suppressed collision frequencies in a supersonic jet and typical (<10 μW) difference frequency power levels. The Gaussian component for each transition arises from residual Doppler broadening in the planar expansion, and is determined from an unconstrained least squares fit (floating both Gaussian and Lorentzian components) to selected strong transitions in the $\nu_2+\nu_6$ $K=1\leftarrow 0$ band. For the weaker $\nu_1+\nu_3$ $K=0\leftarrow 0$ combination band observed under identical slit jet conditions, this Doppler component is scaled linearly by the small (2.9%) fractional increase in origins between $\nu_1+\nu_3$ and $\nu_2+\nu_6$. High resolution scans (7.5 MHz step size, signal averaging 4–6 pulses) over transitions for several J levels in a given VRT band are fit separately. No statistically significant J dependence is found, though a clear sensitivity to the tunneling symmetry is demonstrated. The Lorentzian components reported in Table IV therefore represent an average over transitions into several J states observed in a given VRT band.

The predissociation linewidths for $\nu_2+\nu_6$ and $\nu_1+\nu_3$ are qualitatively similar to the linewidths for ν_2 and ν_1, respectively (see Table IV). Nonetheless, a smaller effect due to initial intermolecular excitation is also observed and follows a trend first identified[16] in the combination bands associated with ν_4 and ν_5; intermolecular excitation *increases* predissociation rates in ν_1 and *decreases* these rates in ν_2. Specifi-

TABLE IV. Vibrational predissociation linewidths (in MHz) for HF dimer. The A^+ and B^+ symmetry labels refer to $\Gamma_{\text{vib-tun}}$ in the upper vibrational state (all $K=0$ except $K=1$ for $\nu_2+\nu_6$).

	$\Delta\nu_{pd}$/MHz			
	Experiment		Theory[a]	
$\Gamma_{\text{vib-tun}}$	A^+	B^+	A^+	B^+
ν_1	6.4 (5)[b]	9.5 (5)[b]	4.9	4.1
$\nu_1+\nu_3$	90(20)	60(20)		
$\nu_1+\nu_4$	25(5)	40(8)	8.2	12
$\nu_1+\nu_5$	20(5)	45(8)	5.2	5.5
$\nu_1+\nu_6$				
ν_2	330 (30)[b]	330 (30)[b]	48	51
$\nu_2+\nu_3$				
$\nu_2+\nu_4$		300 (50)	85	83
$\nu_2+\nu_5$	270 (20)	270 (20)	29	38
$\nu_2+\nu_6$	240 (20)[c]	250 (20)[c]		

[a]$\Delta\nu_{pd}$ is calculated using the predissociation lifetimes reported in Refs. 68 and 69.
[b]Reference 13.
[c]The ν_6 states are odd parity so the symmetry labels are $\Gamma_{\text{vib-tun}}=A^-$ and B^-, respectively.

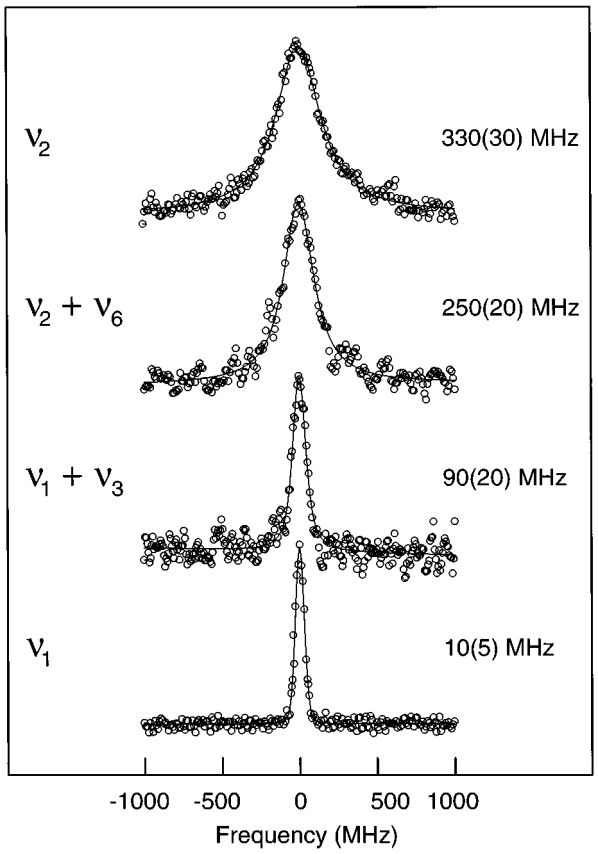

FIG. 5. Four representative VRT lineshapes for the ν_1 and ν_2 intramolecular fundamentals, and the $\nu_2+\nu_6$ and $\nu_1+\nu_3$ combination bands of $(HF)_2$. The circles are the experimental data, and the lines are the simulated Voigt profiles which deconvolute the inhomogeneous and homogeneous (lifetime) contributions to the broadening. The ν_1 and ν_2 examples are $\Gamma_{\text{vib-tun}}=B^+$ states while the $\nu_1+\nu_3$ and $\nu_2+\nu_6$ line shapes are for $\Gamma_{\text{vib-tun}}=A^+$, B^- states, respectively. The mode specificity in the intramolecular fundamentals is predominantly maintained in the combination bands, however there are also clear effects due to ν_3 or ν_6 excitation.

cally, the predissociation broadening for the two tunneling states of $\nu_1+\nu_3$ are nearly tenfold greater than the predissociation broadening in ν_1, whereas the predissociation linewidths for both tunneling components of $\nu_2+\nu_6$ are 25% smaller than the analogous $K=0$ linewidths in ν_2 (the ν_2 $K=1$ predissociation rates have not yet been reported). This is particularly evident in Fig. 5, which shows representative lineshapes for the $\nu_2+\nu_6$ and $\nu_1+\nu_3$ combination bands along with the ν_1 and ν_2 fundamentals. The strong ν_1/ν_2 mode specific predissociation rates are evident by comparing the fundamental lineshapes in Fig. 5, but the weaker effect of intermolecular excitation is also clearly visible.

This intermolecular dependence of the predissociation broadening suggests the following interpretation. In the absence of intermolecular excitation, the two intramolecular modes are best described as nearly local modes with the vibrational energy either in the ''free'' or ''bound'' HF subunit. Consequently, these two vibrations have dramatically different predissociation rates with ν_2 (predominantly ''bound'') predissociating 30–50-fold faster than ν_1 (predominantly ''free'').[13] Indeed, it has been postulated that predissociation only occurs from the ''bound'' HF-stretch, and thus the difference in predissociation rates is a measure of the local mode character of the two intramolecular modes.[66] Intermolecular excitation, however, tends to weaken the hydrogen bonding interactions that lift the degeneracy of the two HF stretches for completely decoupled HF subunits. Therefore, small changes in the ''bound'' versus ''free'' character of the two intramolecular modes induced by *intermolecular* excitation could lead to large fractional differences in the observed predissociation rates from combination states.

From a theoretical perspective, Zhang, Bacic, and co-workers[68] have presented 4-D time independent golden rule calculations of the vibrational predissociation lifetimes for $(HF)_2$ on the SQSBDE surface. Initial calculations for ν_1 and ν_2 have recently been extended to combination states[69] of the intramolecular modes with ν_4 and ν_5, these results are also shown in Table IV for comparison. The *qualitative* agreement between experiment and theory is quite good, i.e., the calculated values do reproduce the broader predissociation widths for ν_2 vs ν_1 excitation. In addition, the increased broadening in the $\nu_1+\nu_4$ and $\nu_1+\nu_5$ combination states relative to the ν_1 state, and decreased broadening between the $\nu_2+\nu_5$ and ν_2 states are also correctly predicted. However, the trend between $\nu_2+\nu_4$ and ν_2 is not well reproduced, i.e., the $\nu_2+\nu_4$ predissociation linewidth is broader than ν_2, in clear disagreement with experiment. At a more *quantitative* level of comparison, the predissociation linewidths are systematically underpredicted, typically a factor of 2–8 smaller than the experimental values. Extension of these vibrational predissociation calculations to $\nu_1+\nu_3$ and $\nu_2+\nu_6$ would be useful since these two modes display larger intermolecular effects on the predissociation broadening. It also would be interesting to examine the intramolecular dependence of the eigenfunctions calculated in the 6-D resonance state calculations[45] to determine if the present interpretation that

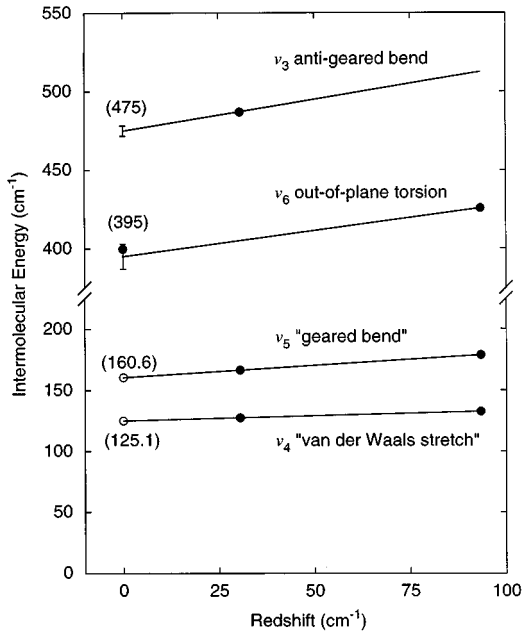

FIG. 6. Plot of all the experimentally observed (filled circles) intermolecular energies as a function of intramolecular redshift. Both the ν_4 and ν_5 energies have been reported previously (Ref. 16) and are used to make extrapolations (see the text for details) of the far-ir (i.e., zero redshift) intermolecular energies of ν_3 ($K=0$) and ν_6 ($K=1$).

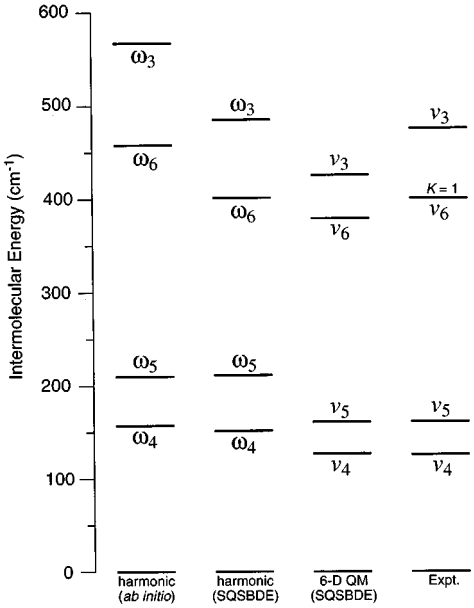

FIG. 7. Energy level diagram of the $(HF)_2$ intermolecular fundamental energies measured in the far-ir (ν_6, $K=1$) and extrapolated from the current near-ir data (ν_3,ν_4,ν_5, $K=0$). Included for comparison are harmonic estimates of the intermolecular energies based on (i) recent *ab initio* calculations (Ref. 71) and (ii) the SQSBDE potential (Ref. 39). The intermolecular energies predicted from 6-D quantum calculations (Ref. 44) on the SQSBDE potential surface are also included. The agreement between the calculated values and experiment is excellent, except for the ν_3 the ''high frequency'' antigeared bend.

the changes in the predissociation rates in combination states result from changes in the intramolecular local mode character of ν_1 and ν_2. Indeed, vibrational predissociation calculations provide a particularly demanding test of the potential accuracy, especially for the anisotropy of the repulsive wall and the coupling between inter- and intramolecular degrees of freedom. Table IV suggests that the SQSBDE surface does a reasonably good job at capturing predissociation trends, though it considerably underpredicts the magnitude of inter/intramolecular mode coupling.

C. Extrapolation to intermolecular vibrational fundamentals

One primary goal of the present study is to provide detailed high-resolution measurements for *all* intermolecular degrees of freedom in a prototypic hydrogen bonded complex. Since the current study necessarily observes these vibrations via combination bands built on high frequency intramolecular HF-stretching modes, the most direct and rigorous comparison with theory would be via full 6-D ''resonance'' calculations on exactly these combination states. However, these resonance calculations are computationally demanding and, furthermore, can not isolate discrepancies due explicitly to inter- versus intramolecular regions of the potential surface. Thus a useful alternative strategy would be to develop a procedure for extrapolating intermolecular frequencies from the available combination band data to the ground (i.e., $\nu_1=\nu_2=0$) state, thus predicting the vi-

TABLE V. Intermolecular frequencies determined from the near-ir combination bands used to extrapolate the far-ir intermolecular fundamentals. The majority of far-ir values are based on extrapolations of excited K-state measurements, except for the $K=1$ ν_6 state. The results of exact 6-D quantum calculations based on the two analytical $(HF)_2$ PES's are also included for comparison. All values are in cm^{-1}.

Vib	K	ν_2	ν_1	Extrapolated	far-ir	SQSBDE[a]	BJKLK[b]
ν_3	0		487.0153(4)	475(3)		425.30	430.29
ν_4	0	132.6160(19)	127.5726(2)	125.1(1)	125(5)[c]	126.37	123.59
ν_5	0	178.6673(4)	166.5232(2)	160.6(6)	161(5)[d]	160.58	163.37
ν_6	0				375(5)[c]	378.72	380.76
ν_6	1	425.6897(5)		395(8)	399.787(1)[e]	402(4)[c]	

[a]Reference 44.
[b]References 46 and 47.
[c]Reference 39.
[d]Reference 8.
[e]Reference 6.

brational frequencies that would be observed in a far-ir experiment. In essence, this amounts to a relatively small correction for off-diagonal anharmonicity between the inter- and intramolecular degrees of freedom. These results can then be compared with *exact* 6-D calculations on a trial potential surface for intermolecular modes *without* ν_1/ν_2 excitation, and thereby probe the intermolecular dependence of the potential surface in isolation.

To make improved predictions of the ν_3 and ν_6 fundamental frequencies from combination band data, we take advantage of the strong correlation between (i) the intermolecular frequency determined from neglecting off-diagonal anharmonicity (i.e., $\nu_{\text{inter}} \approx \nu_{\text{comb}} - \nu_{\text{intra}}$) and (ii) the intramolecular redshift of the HF-stretching mode on which the combination band is built. Physically, this correlation arises because these redshifts are a direct measure of the increase in hydrogen bond strength upon ν_1/ν_2 excitation, which in turn slightly increases the intermolecular vibrational frequencies. Indeed, this correlation has been shown[16] to be remarkably linear for ν_4 and ν_5 in $(HF)_2$, and in all cases where this can be tested against experiment, the fractional intermolecular frequency shifts in $(HF)_2$ and $(DF)_2$ prove to be largely independent of the intermolecular mode.

This motivates the following simple model, whereby the set of all near-ir measurements for which intermolecular frequencies are obtained from both ν_1 and ν_2 combination bands are least squares fit to a single parameter expression,

$$\frac{E_{\text{inter}}^{\nu_{1,2}} - E_{\text{inter}}^{\text{g.s.}}}{E_{\text{inter}}^{\text{g.s.}}} = b(\nu_{\text{HF}} - \nu_{1,2}). \tag{2}$$

In Eq. (2), $E_{\text{inter}}^{\nu_{1,2}}$ is the intermolecular energy determined from the ν_1 or ν_2 combination band and $E_{\text{inter}}^{\text{g.s.}}$ is the intermolecular frequency in the ground HF-stretching state (i.e., for zero redshift). The results of this model are plotted in Fig. 6 and presented in Table V for all four intermolecular modes. Where comparison data is available, this plot indicates essentially quantitative agreement with experiment. For example, the 395(8) cm^{-1} value for ν_6 $(K=1)$ obtained from the model extrapolation agrees with far-ir experimental measurement of 399.787(1) cm^{-1} to well within the uncertainty of the fit, suggesting this as a useful algorithm for predicting far-ir intermolecular frequencies for a high-resolution spectral search.

In the case of the ν_3 antigeared bend mode, extrapolation of the combination band data leads to a $J=K=0$ value of 475(3) cm^{-1} (the smaller uncertainty in this estimate for ν_3 is due to the fact that the experimental near-ir value is from a ν_1 based combination band with a 2–3-fold smaller redshift than ν_2 based combination bands). This is the only intermolecular mode for which neither far-ir nor near-ir data had been previously available, and thus completes the set of 4 intermolecular modes. For both the ν_4 and ν_5 vibrations, reliable values already exist for the $J=K=0$ energies; as evident in Table V, the agreement between experimental far-ir results and the extrapolated values is excellent. The ν_6 out-of-plane intermolecular mode can only be observed in perpendicular bands in both the far and near-ir, and thus direct spectroscopic data is only available for $K=1$. The resulting three $K=0 \leftarrow 0$ (ν_3, ν_4, ν_5) and one $K=1 \leftarrow 0$ (ν_6) intermolecular frequencies are plotted in Fig. 7.

Due to the predominant role of large amplitude motion on an anharmonic potential surface any quantitative comparison between theory and experiment requires that the large amplitude intermolecular dynamics be included. The results of such full 6-D calculations on the SQSBDE[44] and BJKLK[46,47] surface are also reported in Table V. It is apparent that even though the SQSBDE surface has been empirically adjusted to reproduce the experimentally observed dissociation energy (D_0) of the complex, the predictions from both potential surfaces are in substantial agreement with one another. However, as illustrated in Fig. 7, the importance of anharmonic corrections in these full 6-D calculations can be appreciated by comparing the harmonic (ω) and anharmonic (ν) intermolecular frequencies both calculated on the SQSBDE surface.

As discussed previously, the frequencies of the ν_4 and ν_5 intermolecular vibrations are well reproduced by both sets of 6-D calculations, yet significant discrepancies between experiment and theory have been identified by quantities sensitive not only to the eigenvalue but the eigenfunction as well.[16] In the case of the ν_6 vibration, only the *excited* $K=1$ state has been observed, so that the experimental ν_6 frequency can not be compared directly with the exact 6-D theoretical results for $J=K=0$. Therefore, comparison is made with 6-D quantum Monte Carlo calculations performed on the SQSBDE surface which have been approximately extended to excited J,K rotational levels using the clamped coordinate quasiadiabatic channel method.[39] The 402 cm^{-1} predicted value of ν_6 $K=1$ is in excellent agreement (0.5%) with the far-ir value, which suggests that out-of-plane motion on the PES is modeled with reasonable accuracy. In addition, extrapolated values of ν_6 $K=0$ have been made based on far-ir measurements[39] which allow the rotationless ν_6 vibration to be estimated at 375(5) cm^{-1} (see Table V); this is important for calculating the zero-point energy associated with the intermolecular modes.

The largest discrepancy between theory and experiment is on the frequency of the ν_3 fundamental (see Fig. 7). The 475(3) cm^{-1} value is *underestimated* on both PES's by approximately 10%. This is by far the largest deviation measured for all the intermolecular modes and thus warrants further efforts to identify the possible reason for the failure. For example, the ν_3 eigenfunction calculated in the 6-D quantum calculations does not have the nodal pattern expected for a pure antigeared bend, but also has appreciable geared bend character.[44] As discussed previously, this could be due to significant angular–angular and radial–angular coupling in the PES, resulting in partial mixing between antigeared bend and overtone/combination levels of the geared bend and van der Waals stretch states.

This interpretation that the ν_3 state on the SQSBDE surface has appreciable geared bend character is certainly consistent with the large predicted increase (34-fold) in the tunneling splitting for this excited intermolecular state. In contrast, the tunneling splitting observed experimentally for

the $\nu_1+\nu_3$ state is quite small, and does not reflect a large increase relative to the ν_1 state splitting. The large increases in the tunneling splitting for the lower energy ν_4 and ν_5 excited states was interpreted as evidence of appreciable geared bend character for both these states, and thus considerable projection along the tunneling coordinate. The disagreement between theory and experiment for the antigeared bend therefore may result from *too much* geared bend character in the predicted ν_3 state, which has the effect of increasing the tunneling splitting and possibly lowering the intermolecular energy. Instead, the ν_3 experimental data is more consistent with a higher energy state that has little geared bend character at all.

D. An empirical estimate of the hydrogen bonding energy in $(HF)_2$

The set of intermolecular fundamental vibrations for $(HF)_2$ described above can be used to provide an improved empirical estimate of D_e. This is a particularly problematic issue in weakly bound systems, and highlights the difficulty of making detailed comparisons between full quantum theory and experiment. Since spectroscopic measurement obtains differences in experimental eigenvalues, any rigorous comparison necessarily requires that (i) a *global potential surface* be constructed, and (ii) the corresponding multidimensional quantum mechanics be solved exactly on this surface with no dynamical approximation. The first step of generating a global potential surface from *ab initio* methods is a major challenge, with obvious tradeoffs between quality of calculation per geometry and the number of configurations sampled. However, even given such a global potential surface, this second step is not currently feasible for a hydrogen bonded cluster with more than four atoms; for a relatively ''simple'' four atom species such as $(HF)_2$, this $3N-6=6$ dimensional calculation already represents the current state-of-the-art.

A simpler alternative, at least from a theoretical perspective, is to perform a limited number of much higher level *ab initio* calculations to obtain D_e, the binding energy of the global minimum with respect to dissociation. For example, there have been recent *ab initio* calculations by both Dunning[70] and Schaefer[71] on $(HF)_2$, which provide new values for D_e treating correlation effects at a level much higher than was possible in the earlier work of Kofranek *et al.*[31] and on which both the BJKLK and SQSBDE analytical surfaces are explicitly based. Since D_e is not an experimental observable, however, we must use spectroscopic methods to provide quantum corrections to the true experimental observables such as D_0. The present high-resolution combination band data on HF dimer, and in particular the measurement of the ν_3 antigeared bend, make this possible.

The essential difficulty associated with a spectroscopic determination of D_e is the amount of zero-point energy associated with the intermolecular modes (E_{inter}). As first described by Pine,[12] the well depth (D_e) is obtained from the dissociation energy (D_0) by

$$D_e = D_0 + E_{\text{inter}} - \Delta E_{\text{intra}}, \tag{3}$$

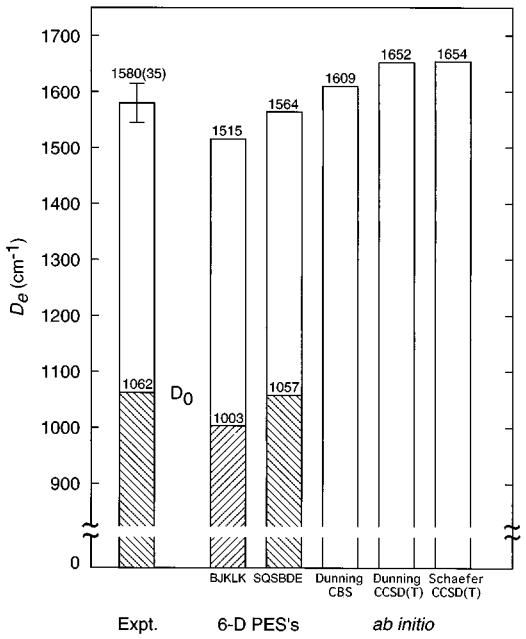

FIG. 8. A bar chart of the estimates of the dissociation energy (D_0, shaded) and hydrogen bond energy (D_e) of $(HF)_2$. The experimental values are compared with the well depths and calculated dissociation energies of the BJKLK and SQSBDE potentials, along with results from two recent *ab initio* calculations (see the text for details).

where E_{inter} is the sum of zero-point energies of the intermolecular vibrations in the dimer, and ΔE_{intra} is the change in the zero-point energy associated with the high frequency HF stretches. The dissociation energy D_0 of $(HF)_2$ has been accurately determined to be 1062(1) cm^{-1} by the photofragmentation studies of Miller and co-workers.[14,72,73] The change in the *harmonic* zero-point energies of the two high frequency HF stretches upon dimerization can be adequately approximated from the known vibrational frequencies of the dimer and monomer, i.e., $\Delta E_{\text{intra}} \approx [\nu_{\text{HF}} - (\nu_1+\nu_2)/2] = 61.9313(3)$ cm^{-1}. Since extensive overtone series have been observed in both the monomer[74,75] and the dimer,[17–19] an even better approximation that takes *anharmonic* effects into account is possible; if one treats the monomer (ν_{HF}) and dimer (both ν_1 and ν_2) modes as Morse oscillators, the magnitude of this additional anharmonic term is -7.1 cm^{-1}. This yields a net value for the intramolecular zero-point contributions of $\Delta E_{\text{intra}} = 54.8$ cm^{-1}, with an uncertainty conservatively estimated at 1 cm^{-1}.

By far the largest correction in obtaining D_e from D_0 is associated with zero-point energy in the low-frequency intermolecular modes, the frequencies of which have now all been measured or reliably estimated for the ground intramolecular state. The challenge is to use the experimentally observed fundamental frequencies to predict accurately the amount of intermolecular zero-point energy, which we estimate via the following method. We calculate the 4-D intermolecular zero-point energy directly on a trial potential surface by solving for the energy of the intermolecular ground state with respect to the minimum on the potential. For HF monomers clamped at vibrationally averaged bond lengths

($r_{HF}=1.767\ a_0$), the calculated intermolecular zero-point energy on the SQSBDE potential is $E_{inter}^{theory}=547.63\ cm^{-1}$. If we then assume that the *ratio* of the true zero-point energy to the sum of the intermolecular fundamental frequencies is adequately reproduced by the SQSBDE surface, the experimental zero-point energy can be obtained from

$$\frac{E_{inter}^{expt}}{\Sigma_i \nu_i^{expt}}=\frac{E_{inter}^{theory}}{\Sigma_i \nu_i^{theory}} \tag{4}$$

The ratio of the zero-point energy to the sum of 4-D intermolecular frequencies is calculated to be 0.5028 on the SQSBDE surface, leading to an *experimental* estimate of $E_{inter}^{expt}=571.0\ cm^{-1}$. For comparison, the BJKLK surface predicts a ratio of 0.5097, but the near quantitative agreement for this ratio on both potentials is more an indication of the similarities between the two surfaces than a measure of the accuracy of this method for predicting the true intermolecular zero-point energy. The experimental value of E_{inter}^{expt} is only slightly larger than the theoretical value calculated on the SQSBDE surface because this surface reproduces 96% of the sum of experimental intermolecular frequencies [see Eq. (4)]. Thus our best estimate for D_e is 1580(35) cm^{-1}, where the uncertainty is dominated by the accuracy of the zero-point ratio (0.5028) used to scale the experimental results. We conservatively estimate a possible $\pm 5\%$ error in this zero-point ratio based on how well the SQSBDE surface reproduces the sum of intermolecular frequencies. However, this zero-point ratio and the corresponding value of D_e should be tested and improved as further refinements of the potential surface become available. The D_e value determined from the present analysis is compared with selected theoretical predictions in Fig. 8.

The D_e values on both the BJKLK and SQSBDE potentials are smaller than the present experimental estimate. These potentials are constructed from the *ab initio* calculations of Kofranek *et al.*[31] using the coupled pair functional method, with additional *ab initio* points added by Bunker *et al.*[29] using the closely related averaged coupled pair functional level of theory. The BJKLK surface predicts[46,47] $D_e=1515\ cm^{-1}$ and $D_0=1003\ cm^{-1}$, both of which are significantly lower than experiment. The agreement between theory and experiment for D_e is much improved on the semiempirical SQSBDE surface (see Fig. 8), which is mainly due to the fact that this version of the surface was adjusted to reproduce D_0. However, a closer inspection of the SQSBDE potential reveals the excellent agreement for D_e is partially fortuitous. In particular, the change in high frequency HF-stretching zero-point energy is underestimated[76] on the SQSBDE potential [$\Delta E_{intra}\approx 3958-(3940.6+3896.4]/2=39.5\ cm^{-1}$) by nearly 22 cm^{-1} while the intermolecular zero-point energy is also approximately 23 cm^{-1} (571.0–547.6 cm^{-1}) too small. Thus, on the SQSBDE surface these two errors nearly cancel [see Eq. (3)], leaving the predicted value of D_e within 1% of experiment. This difficulty in correctly modeling the intra/intermolecular dependence of the full 6-D potential is fully appreciated by the authors of the SQSBDE surface,[77] and indeed is the focus of current efforts to generate improved semiempirical $(HF)_2$ potentials.

Recently, Peterson and Dunning reported the geometry and hydrogen bond energy of $(HF)_2$ using several theoretical methods including Moller–Plesset perturbation and coupled cluster theories with large correlation consistent basis sets.[70] They also investigated the effect of basis set superposition error on the $(HF)_2$ binding energy using the standard counterpoise (CP) correction method.[78] The CP corrected D_e values are consistently lower than the uncorrected values for a given basis set, but these differences decrease regularly with increasing quality of the basis set. At their highest level of theory using coupled clusters singles and doubles with perturbative estimates of triple excitations [CCSD(T)] and the largest basis set, the CP corrected (uncorrected) value of D_e is 1564 cm^{-1} (1652 cm^{-1}). However, Peterson and Dunning have taken these calculations one step further; from the systematic dependence of D_e on increasing the quality of the basis set, extrapolation to the ''complete'' basis set limit (CBS) predicts $D_e=4.60$ kcal/mol$=1610\ cm^{-1}$ (see Fig. 8). Thus for the CCSD(T) calculations the CP corrected D_e values approach the CBS limit from below while the uncorrected values approach it from above, yet as they should, both predict the same CBS limit. This value is now in good agreement with experiment, yet is still on the high side of the stated uncertainty in D_e and in principle may indicate some small residual discrepancy. Nevertheless, the agreement between *ab initio* theory and experiment is already verified on the $\leqslant 0.1$ kcal/mol level, which in the field of hydrogen bonding interactions represents a significant accomplishment.

In a later *ab initio* study by Schaefer and co-workers[71] at the CCSD(T) level of theory using similarly large basis sets, D_e was predicted to be 1654 cm^{-1} without CP correction, i.e., well within 0.01 kcal/mol of the comparable prediction of Peterson and Dunning. These calculations were not corrected for basis set superposition error so further comparison of D_e with experiment is not possible. However, Schaefer and coworkers presented harmonic vibrational frequencies and ir intensities using the CCSD(T) method and a series of large basis sets. These calculations predict ω_6 and ω_3 at *higher* frequencies than the corresponding harmonic predictions on the SQSBDE surface (the ω_4 and ω_5 predictions are nearly identical to the SQSBDE values, see Fig. 7). As discussed earlier, harmonic predictions of the intermolecular modes cannot be quantitatively compared with experiment, but estimates of the anharmonic frequencies can be made from the *ab initio* harmonic frequencies scaled by anharmonicity $\omega_e x_e/\omega_e$ ratios calculated on the SQSBDE surface. Specifically, we theoretically estimate the anharmonicity ratio ($\omega_e x_e/\omega_e$) associated with each intermolecular mode in the Morse oscillator approximation by using the harmonic[39] and numerically exact[44] 6-D frequencies for each intermolecular mode calculated on the SQSBDE potential surface. With this procedure to scale the Schaefer results, ν_3 and ν_6 are predicted at 507(10) cm^{-1} and 436(10) cm^{-1}, respectively. This value of ν_6 is significantly greater (16%) than the experimentally extrapolated value (see Table V), which may

reflect inaccuracies in the *ab initio* results. The value of ν_3 on the other hand is in substantially better agreement (4% vs -10%) with the experimental value than either of the ν_3 frequencies calculated on the analytical surfaces.

As a final test of potential surfaces, one area that deserves further theoretical investigation is the prediction of ir intensities in $(HF)_2$. For example, early 4-D quantum calculations of far-ir intensities in $(HF)_2$ by Clary and co-workers[61] based on the BJKLK potential surface predict the anti-geared bend (ν_3) to be a factor of 15 weaker than the geared bend (ν_5) in oscillator strength. This prediction of a stronger ν_5 vs ν_3 mode is actually in good qualitative agreement with experiment ($I_{\text{geared}}/I_{\text{anti-geared}}=17$), whereas the most sophisticated *ab initio* calculations predict ω_5 to be 1.13-fold *weaker* than ω_3.[71] In addition, several of the intermolecular modes are observed in combination with *only one* of the intramolecular modes; for example, the $K=1\leftarrow 0$ band of $\nu_2+\nu_6$ is quite strong but the corresponding $K=1\leftarrow 0$ $\nu_1+\nu_6$ band must be down in oscillator strength by at least 200-fold to avoid detection at our current sensitivities. Theoretical predictions of combination band intensities using the 6-D quantum methods may provide insight into the intensity anomalies identified in $(HF)_2$. These types of *eigenfunction* sensitive calculations provide particularly demanding tests of the current hydrogen bond potentials. Furthermore, since intra–intermolecular coupling plays a key role in determining the transition strength of combination bands, such calculations and comparisons offer a crucial level of information to construct the next generation of full 6-D $(HF)_2$ potential surfaces.

V. SUMMARY

In this paper we report the measurement of near infrared VRT spectra for $(HF)_2$ which access excited states in both the out-of-plane torsion and antigeared bend coordinates for excited HF-stretch vibrational states. The donor–acceptor tunneling splitting is not strongly increased in the ν_3 or ν_6 intermolecular excited states, which indicates that neither of these two intermolecular modes is significantly coupled with the tunneling coordinate. Predissociation broadening in the combination bands is dominated by intramolecular mode specificity, yet there is also an appreciable dependence on the intermolecular mode as well. This is qualitatively consistent with a simple physical model of the influence of intermolecular excitation on the mixing between the ''free'' and ''bound'' HF-stretch character of the intramolecular modes.

With the observation of $\nu_2+\nu_6$ and $\nu_1+\nu_3$, all four intermolecular modes have now been detected in the near-ir via combination bands. The near-ir data have been used to make predictions of the intermolecular fundamental frequencies, which in turn permit a rigorous evaluation of the current potentials. Excellent agreement is obtained for all the intermolecular frequencies except for the antigeared bend (ν_3), which is significantly underpredicted (-10%) by 6-D quantum calculations. Similarly, tunneling splittings for intermolecular excited states are well predicted except for the ν_3 excited state. In addition, knowledge of all four intermolecular modes in $(HF)_2$ permit the hydrogen bond energy (D_e) to be experimentally estimated at 1580(35) cm^{-1} (4.52(10) kcal/mol). Agreement with recent high level *ab initio* calculations of D_e is within the 35 cm^{-1} (0.1 kcal/mol) experimental uncertainty. However, these high level *ab initio* calculations have thus far only been performed for a limited range of dimer geometries near equilibrium. It remains an outstanding challenge whether a sufficiently dense grid of points can be obtained at this level of theory, which would stimulate the development of a significantly improved ''benchmark'' potential surface for this prototypic hydrogen bonded system.

ACKNOWLEDGMENTS

Financial support for this research from the National Science Foundation is gratefully acknowledged. D.T.A. also wishes to thank the National Research Council for a postdoctoral fellowship through NIST. In addition, we would like to thank Dr. J. T. Farrell, Jr. for considerable assistance in the early stages of these experiments.

[1] T. R. Dyke, B. J. Howard, and W. Klemperer, J. Chem. Phys. **56**, 2442 (1971).
[2] W. J. Lafferty, R. D. Suenram, and F. J. Lovas, J. Mol. Spectrosc. **123**, 434 (1987).
[3] B. J. Howard, T. R. Dyke, and W. Klemperer, J. Chem. Phys. **81**, 5417 (1984).
[4] H. S. Gutowsky, C. Chuang, J. D. Keen, T. D. Klots, and T. Emilsson, J. Chem. Phys. **83**, 2070 (1985).
[5] K. von Puttkamer and M. Quack, Mol. Phys. **62**, 1047 (1987).
[6] K. von Puttkamer, M. Quack, and M. A. Suhm, Mol. Phys. **65**, 1025 (1988).
[7] K. von Puttkamer and M. Quack, Chem. Phys. **139**, 31 (1989).
[8] M. Quack and M. A. Suhm, Chem. Phys. Lett. **171**, 517 (1990).
[9] A. S. Pine and W. J. Lafferty, J. Chem. Phys. **78**, 2154 (1983).
[10] A. S. Pine, W. J. Lafferty, and B. J. Howard, J. Chem. Phys. **81**, 2939 (1984).
[11] R. L. Deleon and J. S. Muenter, J. Chem. Phys. **80**, 6092 (1984).
[12] A. S. Pine and B. J. Howard, J. Chem. Phys. **84**, 590 (1986).
[13] A. S. Pine and G. T. Fraser, J. Chem. Phys. **89**, 6636 (1988).
[14] E. J. Bohac, M. D. Marshall, and R. E. Miller, J. Chem. Phys. **96**, 6681 (1992).
[15] E. J. Bohac and R. E. Miller, J. Chem. Phys. **99**, 1537 (1993).
[16] D. T. Anderson, S. Davis, and D. J. Nesbitt, J. Chem. Phys. **104**, 6225 (1996).
[17] M. A. Suhm, J. T. Farrell, Jr., A. McIlroy, and D. J. Nesbitt, J. Chem. Phys. **97**, 5341 (1992).
[18] H.-C. Chang and W. Klemperer, J. Chem. Phys. **98**, 9266 (1993).
[19] H.-C. Chang and W. Klemperer, J. Chem. Phys. **100**, 1 (1994).
[20] D. R. Yarkony, S. V. ONeil, H. F. Schaefer III, C. P. Baskin, and C. F. Bender, J. Chem. Phys. **60**, 855 (1974).
[21] A. E. Barton and B. J. Howard, Faraday Discuss. Chem. Soc. **73**, 45 (1982).
[22] J. F. Gaw, Y. Yamaguchi, M. A. Vincent, H. F. Schaefer III, C. P. Baskin, and C. F. Bender, J. Am. Chem. Soc. **106**, 3133 (1984).
[23] D. W. Michael, C. E. Dykstra, and J. M. Lisy, J. Chem. Phys. **81**, 5998 (1984).
[24] D. W. Schwenke and D. G. Truhlar, J. Chem. Phys. **82**, 2418 (1985).
[25] M. J. Frisch, J. E. Del Bene, J. S. Binkley, and H. F. Schaefer III, J. Chem. Phys. **84**, 2279 (1986).
[26] S. K. Loushin, S. Liu, and C. E. Dykstra, J. Chem. Phys. **84**, 2720 (1986).
[27] J. E. Del Bene, J. Chem. Phys. **86**, 2110 (1987).
[28] M. J. Redmon and J. S. Binkley, J. Chem. Phys. **87**, 969 (1987).
[29] P. R. Bunker, M. Kofranek, H. Lischka, and A. Karpfen, J. Chem. Phys. **89**, 3002 (1988).
[30] G. C. Hancock, D. G. Truhlar, and C. E. Dykstra, J. Chem. Phys. **88**, 1786 (1988).

[31] M. Kofranek, H. Lischka, and A. Karpfen, J. Chem. Phys. **121**, 137 (1988).
[32] D. W. Schwenke and D. Truhlar, G., J. Chem. Phys. **88**, 4800 (1988).
[33] P. R. Bunker, T. Carrington, Jr., P. C. Gomez, M. D. Marshall, M. Kofranek, H. Lischka, and A. Karpen, J. Chem. Phys. **91**, 5154 (1989).
[34] W. Rijks and P. E. S. Wormer, J. Chem. Phys. **90**, 6507 (1989).
[35] P. R. Bunker, P. Jensen, A. Karpfen, M. Kofranek, and H. Lischka, J. Chem. Phys. **92**, 7432 (1990).
[36] P. Jensen, P. R. Bunker, A. Karpfen, M. Kofranek, and H. Lischka, J. Chem. Phys. **93**, 6266 (1990).
[37] S. A. C. McDowell and A. D. Buckingham, Chem. Phys. Lett. **182**, 551 (1991).
[38] S. Rybak, B. Jerziorski, and K. Szalewicz, J. Chem. Phys. **95**, 6576 (1991).
[39] M. Quack and M. A. Suhm, J. Chem. Phys. **95**, 28 (1991).
[40] S. C. Racine and E. R. Davidson, J. Phys. Chem. **97**, 6367 (1993).
[41] M. D. Marshall, P. Jensen, and P. R. Bunker, Chem. Phys. Lett. **176**, 255 (1991).
[42] M. Quack and M. A. Suhm, Chem. Phys. Lett. **234**, 71 (1995).
[43] D. H. Zhang and J. Z. H. Zhang, J. Chem. Phys. **99**, 6624 (1993).
[44] D. H. Zhang, Q. Wu, J. Z. H. Zhang, M. von Dirke, and Z. Bacic, J. Chem. Phys. **102**, 2315 (1995).
[45] Q. Wu, D. H. Zhang, and J. Z. H. Zhang, J. Chem. Phys. **103**, 2548 (1995).
[46] W. C. Necoechea and D. G. Truhlar, Chem. Phys. Lett. **224**, 297 (1994).
[47] W. C. Necoechea and D. G. Truhlar, Chem. Phys. Lett. **231**, 125 (1994).
[48] W. C. Necoechea and D. G. Truhlar, Chem. Phys. Lett. **248**, 182 (1996).
[49] J. K. Gregory and D. C. Clary, Chem. Phys. Lett. **237**, 39 (1995).
[50] J. T. Farrell, Jr., S. Davis, and D. J. Nesbitt, J. Chem. Phys. **103**, 2395 (1995).
[51] E. Riedle, S. H. Ashworth, J. T. Farrell, Jr., and D. J. Nesbitt, Rev. Sci. Instrum. **65**, 42 (1994).
[52] C. M. Lovejoy and D. J. Nesbitt, J. Chem. Phys. **87**, 1450 (1987).
[53] C. R. Pollack, F. R. Petersen, D. A. Jennings, J. S. Wells, and A. G. Maki, J. Mol. Spectrosc. **99**, 357 (1983).
[54] C. Amiot and G. Guelachvili, J. Mol. Spectrosc. **51**, 475 (1974).
[55] H. C. Longuet-Higgins, Mol. Phys. **6**, 445 (1963).
[56] P. R. Bunker, *Molecular Symmetry and Spectroscopy* (Academic, New York, 1979).
[57] M. Quack, Mol. Phys. **34**, 477 (1977).
[58] I. M. Mills, J. Chem. Phys. **88**, 532 (1984).
[59] J. T. Hougen and N. Ohashi, J. Mol. Spectrosc. **109**, 134 (1985).
[60] M. Quack and M. A. Suhm, Chem. Phys. Lett. **183**, 187 (1991).
[61] S. C. Althorpe, D. C. Clary, and P. R. Bunker, Chem. Phys. Lett. **187**, 345 (1991).
[62] S. Davis, D. T. Anderson, and D. J. Nesbitt, J. Chem. Phys. (in press).
[63] E. L. Silbert III, J. Chem. Phys. **93**, 5022 (1989).
[64] G. T. Fraser, J. Chem. Phys. **90**, 2097 (1989).
[65] P. R. Bunker, P. Jensen, and A. Karpfen, J. Mol. Spectrosc. **149**, 512 (1991).
[66] H.-C. Chang and W. Klemperer, J. Chem. Phys. **104**, 7830 (1996).
[67] G. C. Hancock and D. G. Truhlar, J. Chem. Phys. **90**, 3498 (1989).
[68] D. H. Zhang and J. Z. H. Zhang, J. Chem. Phys. **98**, 5978 (1993).
[69] M. von Dirke, Z. Bacic, D. H. Zhang, and J. Z. H. Zhang, J. Chem. Phys. **102**, 4382 (1995).
[70] K. A. Peterson and T. H. Dunning, J. Chem. Phys. **102**, 2032 (1995).
[71] C. L. Collins, K. Morishashi, Y. Yamaguchi, and H. F. Schaefer III, J. Chem. Phys. **102**, 6051 (1995).
[72] D. C. Dayton, K. W. Jucks, and R. E. Miller, J. Chem. Phys. **90**, 2631 (1989).
[73] R. E. Miller, Acc. Chem. Res. **23**, 10 (1990).
[74] R. B. Le Blanc, J. B. White, and P. F. Bernath, J. Mol. Spectrosc. **164**, 574 (1994).
[75] R. S. Ram, Z. Morbi, B. Guo, K.-Q. Zhang, P. F. Bernath, J. Vander Auwera, J. W. C. Johns, and S. P. Davis, Astrophys. J. Suppl. **103**, 247 (1996).
[76] M. Quack and M. A. Suhm, Theor. Chim. Acta **93**, 61 (1996).
[77] M. A. Suhm (private communication).
[78] S. F. Boys and F. Bernardi, Mol. Phys. **19**, 553 (1970).